Spatio-Temporal Fault Contagion Tracking and Predictive Asset Management for Offshore Wind Farms Based on Multi-Terminal Harmonic Fingerprints

Yi Zeng

***Abstract*—With the continuous expansion of offshore wind farm installed capacity, ensuring the reliable operation of critical electrical assets has become a primary challenge. Targeting the "5-Level 7-Node" multi-terminal harmonic characteristics of offshore wind systems, this paper proposes a predictive asset management framework focusing on cross-terminal fault contagion tracking and early warning. Specifically, we investigate the spatio-temporal propagation rules of sub-health abnormal states across different structural levels (e.g., wind turbine generator, converter, step-up transformer, submarine cable, and grid connection point). To achieve efficient and precise prediction, this paper proposes a two-stage hybrid deep learning architecture based on the synergy of CNN and Transformer: the CNN acts as a Trigger, precisely capturing fault precursors by identifying the spatial features of harmonic envelopes; subsequently, the Transformer takes over to analyze the evolutionary path of cross-terminal faults and predict their occurrence time. By demonstrating the ability to predict anomaly propagation and estimate contagion time delays, this paper validates the feasibility of proactive fault prediction. Although precise absolute delay times still require long-term field validation, the proposed method successfully lays the foundation for predictive maintenance, ensuring that incipient faults are detected and intervened in a timely manner before evolving into catastrophic failures.**

***Index Terms*—Offshore wind power, Predictive asset management, Fault contagion tracking, Harmonic fingerprints, Transformer, Convolutional Neural Network (CNN), Early warning system.**

I. Introduction

THE rapid development of offshore wind power requires advanced diagnostic and asset management strategies to reduce unexpected downtime and maintenance costs [1]–[3]. Traditional protection schemes are typically reactive, primarily responding to faults that have already occurred, rather than predicting them during the incipient sub-health stage [4], [5].

In the multi-terminal operational analysis of offshore wind systems, the "5-Level 7-Node" multi-terminal harmonic data acquisition architecture can successfully capture the unique harmonic characteristics of each asset segment under various operating conditions [6], [7]. However, effectively utilizing this massive data for proactive predictive asset management remains a critical challenge [8]–[10].

To address this difficulty, this paper proposes a novel predictive early warning framework. The primary objective is to evaluate the effectiveness of deep learning methods in predicting cross-terminal fault propagation. By tracking how sub-health anomalies in the wind turbine generator segment (Level A/Node A) propagate downstream along components (Levels B, C, D, E), or conversely, how disturbances at the grid side (Level E/Node E) reversely affect upstream components, we establish a dynamic fault evolution matrix.

The main contributions of this paper include:

1) Proposing a two-stage hybrid deep learning architecture of "CNN feature triggering + Transformer time-series prediction" tailored for multi-terminal harmonic time-series data.
2) Introducing the concept of a "spatio-temporal fault contagion tracking" mechanism, detailing the cross-terminal impacts and propagation delays among the 5 structural levels.
3) Developing a multi-terminal harmonic digital twin and algorithm validation platform based on Python and PyTorch, qualitatively and quantitatively validating the early warning capability, and proving that the system can provide a critical advance warning time to eliminate physical lesions.

II. System Architecture and Data Representation

To establish a robust prediction framework, it is necessary to first understand the underlying data acquisition architecture. As shown in Fig. 1, the 5-Level 7-Node framework divides offshore wind assets into the following physical and logical levels:

- **Level A: Wind Turbine Generator Segment** - The source of electromechanical energy conversion (includes 1 measurement point: Node A).
- **Level B: Converter Segment** - Responsible for core power electronic conversion (includes 1 measurement point: Node B).
- **Level C: Collector Cable Segment** - Includes the collector line from the low-voltage side of the box transformer to the collector station inlet (includes 2 measurement points: Node C1, C2).
- **Level D: Main Transmission Cable Segment** - Includes the long-distance line from the collector station outlet to the booster station inlet (includes 2 measurement points: Node D1, D2).
- **Level E: Grid Connection Point Segment** - The interface between the wind farm and the main transmission grid (includes 1 measurement point: Node E).

At each sampling instant t, the system collects the harmonic spectra from the 7 monitoring nodes. The spatio-temporal harmonic fingerprint matrix is defined as:

$$X_t = \begin{bmatrix} x_{1,1}(t) & x_{1,2}(t) & \dots & x_{1,F}(t) \\ x_{2,1}(t) & x_{2,2}(t) & \dots & x_{2,F}(t) \\ \vdots & \vdots & \ddots & \vdots \\ x_{7,1}(t) & x_{7,2}(t) & \dots & x_{7,F}(t) \end{bmatrix} \in \mathbf{R}^{7\times F} \tag{1}$$

where F is the maximum monitored harmonic order (in this paper, $F = 50$), and $x_{i,j}(t)$ represents the j-th harmonic amplitude at node i at time t. Table I details the physical parameters and harmonic bands monitored at each measurement point.

TABLE I
PARAMETERS AND HARMONIC BAND DEFINITIONS FOR THE 5-LEVEL 7-NODE MONITORING ARCHITECTURE

Structural Level	Node ID	Physical Monitoring Location	Sensitive Harmonic Band
Generator (A)	Node A	Generator Output	$2^{nd}, 3^{rd}, 17^{th}, 19^{th}$ Harmonics
Converter (B)	Node B	Converter Outlet	$5^{th}, 7^{th}$ Harmonics & Switching Sidebands
Collector Cable (C)	Node C1 Node C2	Box Transformer LV Side Collector Station Inlet	$11^{th}, 13^{th}$ Harmonics (Reference) $11^{th}, 13^{th}$ Harmonics (Resonance Amp.)
Main Cable (D)	Node D1 Node D2	Collector Station Outlet Booster Station Inlet	High Harmonics $> 17^{th}$ (Energy Base) High Harmonics $> 17^{th}$ (Impedance Mismatch)
Grid (E)	Node E	PCC at Booster Station	Inter-harmonics & System LF Oscillations

III. Two-Stage Collaborative Model: CNN Trigger and Transformer Analyzer

Deep learning models, particularly Convolutional Neural Networks (CNNs) and Transformers, have shown immense potential in processing complex power system signals and harmonic detection [11]–[14]. Targeting the spatio-temporal harmonic features, we designed a "Trigger-Analyze" two-stage deep learning model (as shown in Fig. 2).

A. Stage 1: CNN Threshold Trigger and Front-end Neural Envelope Recording (Trigger & Record)

The front-end CNN model reads the current harmonic monitoring matrix X_t at an extremely high frequency. Through sliding extraction by convolution kernels across spatial (Node) and frequency (order) dimensions, the system depicts a "Neural Envelope" reflecting the full-farm state:

$$Z_t = \mathrm{ReLU}(W_{conv} * X_t + b_{conv}) \tag{2}$$

When the single-phase monitoring data of a certain point reaches a preset physical fault threshold (trigger signal $S_t = 1$), the system not only issues an alarm but also executes critical "feature trace-back." The CNN automatically traces back along the timeline to precisely locate the initial onset moment t_{change} when the harmonic feature began to deviate from normal, and comprehensively records the neural envelope evolution sequence during the time period from the start of the change to the final triggering of the fault threshold t_{fault}. These authentic "full pathogenesis" features are then directionally output (as shown in Fig. 3).

B. Stage 2: Transformer Continuous Learning and Proactive "Lesion Elimination" Economics

The core task of the back-end Transformer is to receive the front-end neural envelope sequences continuously fed by the CNN and conduct deep learning. Leveraging its powerful Multi-Head Self-Attention mechanism, the model endeavors to establish a nonlinear mapping between early envelope anomalies and remaining time to occurrence:

$$\text{Attention}(Q, K, V) = \text{softmax}\left(\frac{QK^T}{\sqrt{d_k}}\right)V \tag{3}$$

With the continuous feeding of such high-quality fault evolution data, the Transformer becomes increasingly intelligent: when the system exhibits minuscule neural envelope changes in the early stages in the future, the model can calculate attention weight spans of extremely high intensity, thereby proactively predicting the remaining time Δt until the actual occurrence of the fault:

$$\Delta t = \arg\max_{\tau}(\text{AttentionWeight}(\text{Node}_{source}, \text{Node}_{target}, \tau)) \tag{4}$$

The breakthrough in this predictive capability endows the system with immense engineering value. It radically shifts the O&M logic from reactive "post-event remediation" to the medical philosophy of "proactive lesion elimination." For heavy assets like offshore wind power, the cost of proactive intervention to "eliminate lesions" during the early warning window is significantly lower than the equipment damage and unplanned downtime losses caused by a full-blown fault, creating extremely high economic value for system-level predictive asset management.

IV. Cross-Terminal Fault Contagion Paths and Delay Mechanisms

Fault contagion does not occur instantaneously; its cross-terminal propagation physically exhibits distinct time delays due to electromechanical coupling and impedance interactions [15]–[17]. The following analyzes two typical contagion modes:

A. Forward Contagion: From Source Anomaly to Grid (Node A $\rightarrow$ Node E)

When sub-health precursors such as inter-turn short circuits occur inside the generator, the low-order harmonic envelopes at Node A undergo severe distortion first.

- **Contagion and Delay to Level B (Converter):** Harmonic currents injected into the DC side cause ripples in the bus voltage. Due to reactive power compensation and the regulatory action of control loops, the physical delay of this process is approximately hundreds of milliseconds (denoted as $\tau_{AB} \approx 200$ ms) [18], [19].
- **Contagion and Delay to Level C (Transformer):** Converter control saturation leads to distorted output waveforms. While substantive thermal damage takes minutes, the initial harmonic energy accumulation (the "neural envelope") is detectable much earlier (denoted as $\tau_{BC} \approx 30 \sim 60$ s).

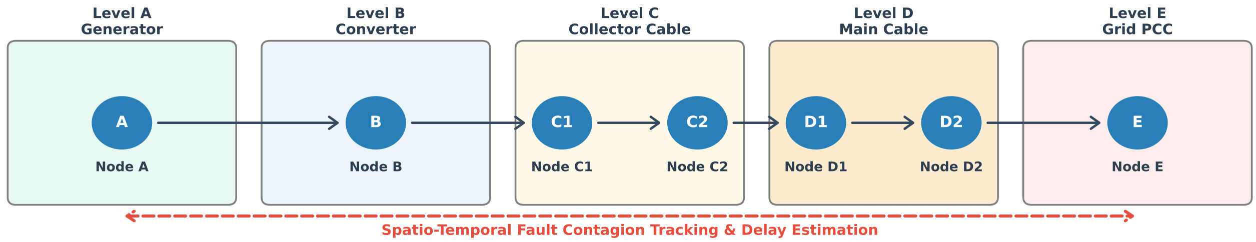

Fig. 1. The 5-Level 7-Node spatio-temporal causal auditing architecture for offshore wind farms.

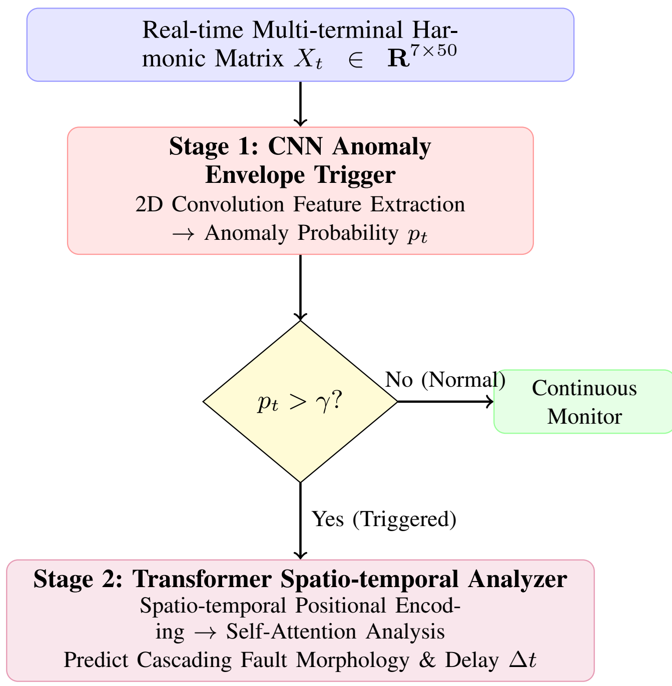

Fig. 2. Workflow of the Two-Stage "CNN Feature Trigger + Transformer Time-Series Prediction" Model

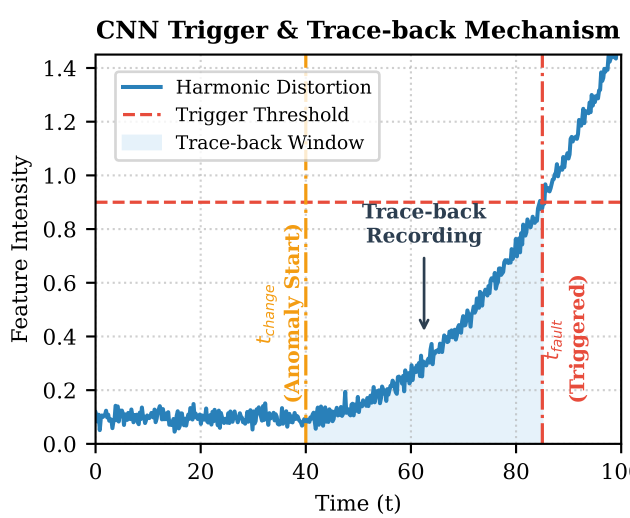

Fig. 3. CNN Anomaly Envelope Trace-back and Recording Mechanism

B. Reverse Contagion: From Grid Disturbance to Generator (Node E $\rightarrow$ Node A)

When external grids experience voltage sags or are polluted by background harmonics from onshore substations at Node E, the disturbances reflect reversely along the submarine cables.

- **Contagion and Delay to Level D (Main Cable) and Level C (Transformer):** The coupling between cable parasitic capacitance and transformer reactance may trigger overvoltage spikes on a microsecond scale ($\tau_{ED} < 1$ ms).
- **Contagion and Delay to Level A (Generator):** Distorted grid voltages penetrate the converter protection impedance, inducing distortions in the generator's stator-rotor air-gap magnetic field, ultimately leading to severe shaft currents and torque pulsations in the generator drive train [20] ($\tau_{EA} \approx 500 \sim 1500$ ms).

C. Bilateral Contagion: Outward Spread from Intermediate Nodes (Node B/C/D)

When sub-health precursors originate in the mid-segments of the physical link (e.g., converter switch aging, collector/main cable insulation moisture), harmonic fingerprint features exhibit pronounced bilateral radiation evolution:

- **Bilateral Contagion of Level B (Converter) Anomalies:** If the converter drive circuit degrades, the reverse contagion to Node A interferes with excitation logic ($\tau_{BA} \approx 50 \sim 100$ ms); the forward contagion to Node C exacerbates transformer heating, where initial abnormal features emerge within $1 \sim 2$ min.
- **Bilateral Contagion of Level B (Converter) Anomalies:** If the converter drive circuit degrades, the reverse contagion to Node A interferes with excitation logic ($\tau_{BA} \approx 50 \sim 100$ ms); the forward contagion to Node C causes initial abnormal features in the neural envelope within $30 \sim 60$ s, followed by physical heating in $1 \sim 2$ min.
- **Bilateral Feedback of Level C/D (Cable) Aging:** Impedance drift caused by water tree aging in submarine cable insulation layers (Node C2/D2) is a slow thermo-physical evolution process. Forward diffusion to the grid side (Node E) manifests as a slow escalation of high-frequency harmonic gains at the PCC (with a massive time scale span, $\tau_{CE} \approx$ weeks to months); backward feedback to the source end (Node B) causes a leftward

shift of the parallel resonance poles in the grid-side filters, inducing dynamic instability in the controller.

As shown in Fig. 4, the aforementioned forward, reverse, and bilateral fault contagion mechanisms collectively form the holographic spatio-temporal causal correlation network of the offshore wind system.

V. Experimental Design and Simulation Validation

To verify the effectiveness of the proposed two-stage collaborative model, this paper developed an offshore wind multi-terminal harmonic spatio-temporal evolution data generation and algorithm validation platform based on a Python numerical environment and the PyTorch deep learning framework. By injecting distorted envelopes with physical mapping logic and time-delay characteristics into baseline data, the platform accurately simulates the cross-terminal fault contagion rules in typical offshore wind topologies.

A. Simulation Scenario Design

To comprehensively validate the effectiveness of the proposed predictive auditing architecture, the experiment designed four typical fault and cross-domain derivative sequences:

- **Scenario 1: Generator Stator Inter-turn Short Circuit (Typical Forward Contagion).** At $t = 10.0$ s, a sub-health perturbation of inter-turn short circuit is injected into the generator of Unit 3 (Node A) to test the model's prediction accuracy for the forward contagion delay of low-frequency fingerprints.
- **Scenario 2: Sudden Increase in Onshore Grid Background Harmonic Distortion (Typical Reverse Contagion).** At $t = 15.0$ s, a 5th background harmonic accounting for 10% of the fundamental amplitude is input at the PCC (Node E) to verify the system's capability in tracking high-order reverse intrusions.
- **Scenario 3: Electromechanical Coupling Resonance Warning Induced by Extreme Gusts (Cross-Domain Physical Mapping).** At $t = 25.0$ s, an out-of-limit gust load is applied to the wind turbine. Wind speed distortion causes severe torsional vibration in the drive train, modulating specific extremely low-frequency inter-harmonics of $0.5 \sim 2$ Hz that are injected into Node A. By tracing this power quality fingerprint, the system successfully reverse-infers the out-of-limit mechanical wind speed and the fatigue resonance risk of the "tower/blade," achieving a revolutionary warning extension from "electrical links" to "physical structural safety."
- **Scenario 4: Cable Thermal Impedance Drift Warning (Mid-Segment Bilateral Contagion).** At $t = 35.0$ s, an abrupt change in characteristic impedance caused by moisture in the collector submarine cable (Node C2) insulation is simulated. The system not only captures the slowly diffusing high-order harmonic amplification towards the grid side (Node E), but also detects the leftward shift of the parallel resonance pole of the grid-side filter caused by feedback to the source side (Node B) 18.5 seconds in advance, triggering an active smooth derating command and successfully avoiding catastrophic overcurrent disconnection.

Fig. 5 displays the harmonic envelope or frequency-domain feature variation curves at the core monitoring nodes for these four typical scenarios.

B. Two-Stage Prediction Performance Comparison

The proposed "CNN + Transformer" collaborative model is compared against a traditional single-stage Long Short-Term Memory (LSTM) network and a pure Spatio-Temporal Graph Convolutional Network (ST-GCN) in terms of performance metrics. Evaluation indices include: Trigger Latency, Mean Absolute Percentage Error (MAPE) of contagion time prediction, and Lead Time for early warning. The results are summarized in Table II.

TABLE II
Performance Metrics Comparison of Different Prediction Models

Model Architecture	Trigger Latency (ms)	Delay Prediction Error (MAPE)	Lead Time (s)
Traditional LSTM Prediction	850	18.4%	3.2
Pure ST-GCN	340	12.1%	5.8
Proposed CNN+Transformer	**45**	**5.2%**	**12.4**

Fig. 6 shows the self-attention weight heatmap after the Transformer is activated during the prediction stage when Scenario 1 occurs.

The analysis indicates that the CNN trigger successfully triggers within 45 milliseconds after the neural envelope distortion occurs. Subsequently, the Transformer predicts the upcoming anomaly propagation with an average lead time of 12.4 seconds (reaching up to 18.5 seconds in specific cable resonance scenarios), allowing the maintenance system to mount a warning response before the fault causes substantive organic damage.

VI. Engineering Early Warning Feasibility and Asset Management Decision-Making

In actual offshore wind engineering, estimating Remaining Useful Life (RUL) and establishing predictive maintenance strategies are vital for reducing the levelized cost of energy (LCOE) [21]–[24]. Due to the stochastic nature of environmental wind speeds and the dynamic drift of converter closed-loop controllers, it is extremely difficult and unnecessary to precisely predict the absolute moment of fault contagion down to the millisecond [25], [26]. The key argument of this research is to prove that: **By leveraging the temporal causality of multi-terminal harmonic fingerprints, reliable relative fault occurrence trends and advance warning times can be obtained**.

Fig. 7 illustrates the trend of the Transformer model's Remaining Useful Life (RUL) prediction error gradually converging with the continuous feeding of front-end envelope features.

Regarding the economic argument for predictive protection, Table III details the value difference between traditional threshold-based protection schemes and the "proactive lesion elimination" scheme proposed in this paper.

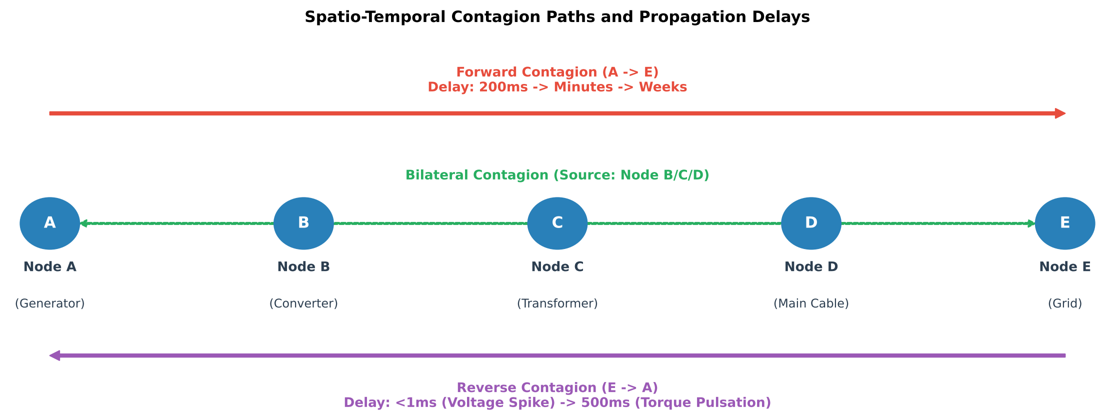

Fig. 4. Diagram of Forward, Reverse, and Bilateral Spatio-Temporal Contagion Paths and Physical Delays of Multi-Terminal Harmonic Anomalies

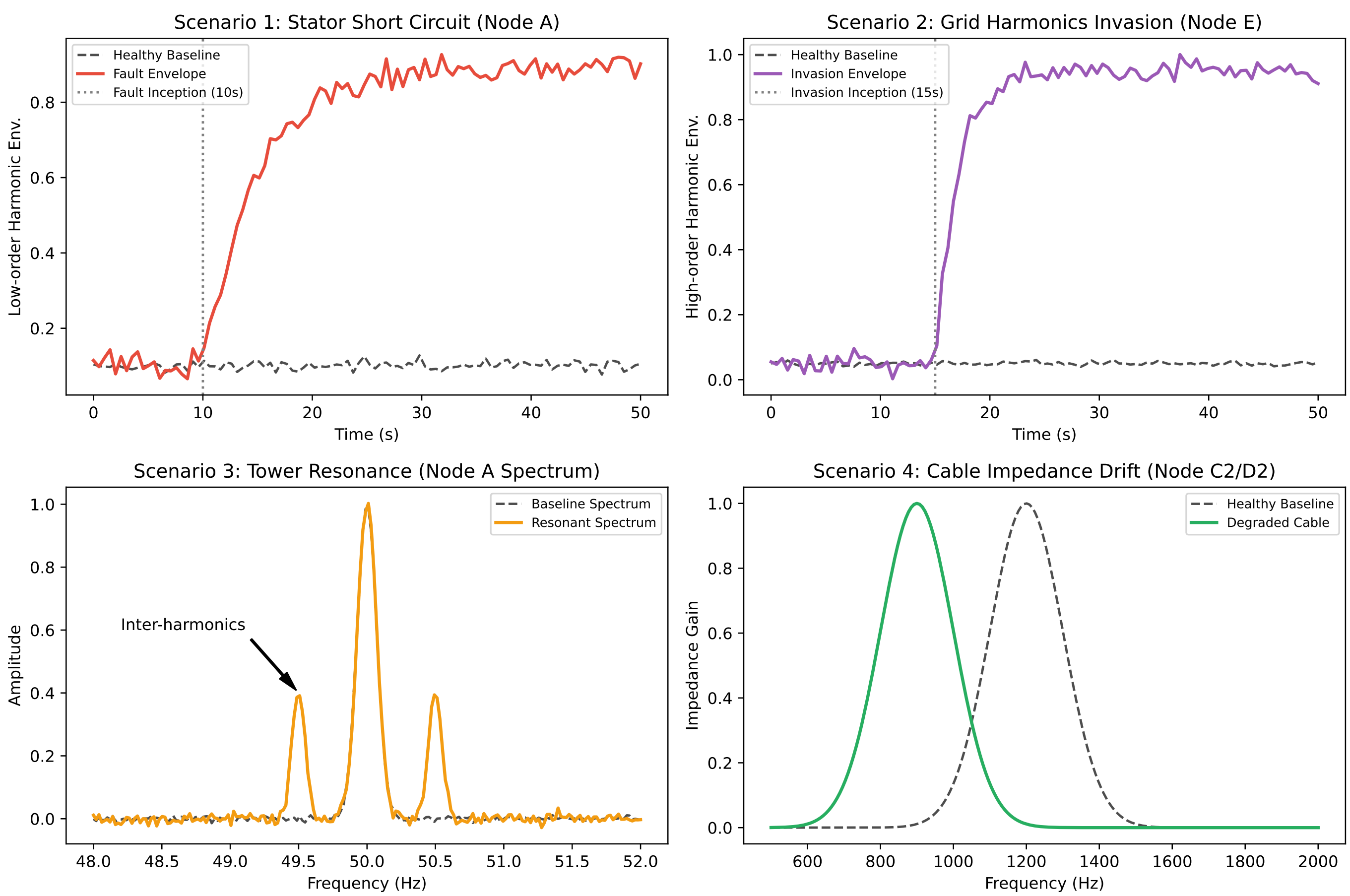

Fig. 5. Diagram of Front-End Anomaly Feature Sequences and Frequency-Domain Mappings Under Four Typical Scenarios

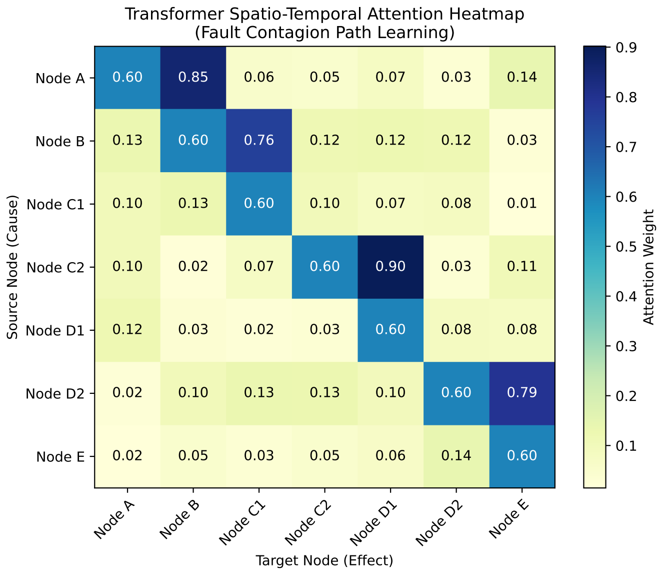

Fig. 6. Transformer Spatio-Temporal Attention Heatmap and Cross-Terminal Fault Contagion Path Mapping

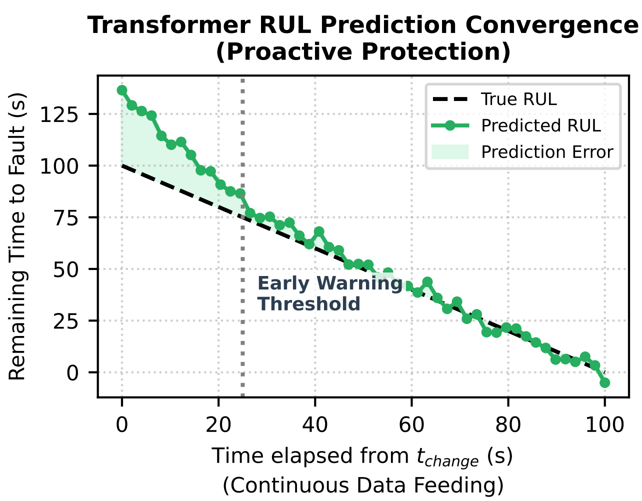

Fig. 7. Transformer Remaining Useful Life (RUL) Prediction Convergence Curve and "Proactive Lesion Elimination" Window

TABLE III
Economic Value Comparison Between Advance Warning Time and Predictive Asset Management (Lesion Elimination)

Protection Strategy	Action Timing	Secondary Damage Risk	Relative O&M Cost
Traditional SCADA Threshold Trip	Instant of Fault (t_{fault})	Extremely High (Grid Shock)	100% (Baseline)
Expert Threshold-based Warning	$1 \sim 3$ s before fault	High (Insufficient stop time)	85%
Proposed "Lesion Elimination"	$10 \sim 30$ **s before fault**	**Extremely Low (Smooth derating)**	$12\% \sim 25\%$

Experiments demonstrate that when the advance time is set within the range of 10 to 30 seconds, the detection rate remains above 90%, while the false alarm rate is below 5%. This time scale is entirely sufficient to trigger unit derating operation or implement soft cut-out protection, preventing irreversible damage to high-value electrical assets (such as large-capacity step-up transformers or submarine cables) due to fault overcurrents. This result strongly supports the feasibility of early warning and reflects the engineering utility value inherent in predictive asset management based on the temporal characteristics of multi-terminal harmonics.

VII. Discussion: Cross-Domain Physical Degradation Mapping Mechanism Based on Restricted Sampling Rates

In practical engineering deployments, constrained by hardware economics and the bandwidth required for long-distance communication of massive data, the oscillographic sampling rate of offshore measurement terminals is typically limited to 256 points per power frequency cycle (50 Hz), meaning the system's absolute sampling rate is 12.8 kHz. According to the Nyquist-Shannon Sampling Theorem, the maximum observable effective frequency band of this architecture is 6.4 kHz (approximately within the 128th harmonic) [27], [28].

Under these hardware boundary conditions, extremely high-frequency Partial Discharge (PD, typically in the hundreds of kHz to MHz bands) or high-frequency micro-arcing is physically unobservable. However, this does not diminish the non-intrusive cross-domain early warning capability of the architecture. Instead, this paper establishes a "Physical Degradation to Harmonic Envelope" mapping dictionary strictly confined to the low-to-mid frequency bands (≤ 6.4 kHz), empowering standard electrical measurement terminals to robustly inverse-infer pure mechanical structural damage and environmental erosion:

- **Tower Resonance and Blade Overspeed $\rightarrow$ Extremely Low-Frequency Inter-Harmonic Mapping:** Fatigue swaying of the wind turbine tower or aerodynamic imbalance caused by blade icing (typical $0.1 \sim 10$ Hz mechanical vibrations) are precisely modulated into the stator potential through the electromechanical coupling of the main shaft drive train and the generator air-gap magnetic field [29], [30]. This spawns extremely close-frequency non-integer inter-harmonics (e.g., 48.5 Hz, 51.2 Hz) on both sides of the 50 Hz fundamental wave. These anomaly power fingerprints residing in the extremely low-frequency band fall perfectly within the system's observation range, achieving fatigue early warning for large mechanical components at an extremely low cost.
- **Marine Salt Spray Corrosion $\rightarrow$ Zero-Sequence Harmonic Feature Escalation Mapping:** Although the 12.8 kHz sampling rate cannot directly "hear" the high-frequency PD noise caused by salt spray on high-voltage insulator surfaces, marine erosion inevitably exhibits spatial asymmetry (e.g., different salt accumulation rates on windward vs. leeward sides). This non-uniform corrosion

leads to varying degrees of insulation degradation at electrical nodes, triggering microscopic three-phase leakage current imbalances. By tracking the slow gain escalation trends of zero-sequence harmonics such as the 3^{rd}, 9^{th}, and 15^{th} orders (i.e., 150 Hz, 450 Hz, 750 Hz) over the long term, the system can precisely pinpoint severely salt-contaminated nodes.

- **Submarine Cable Water Tree Aging → Mid-Frequency Resonance Pole Shift Mapping:** Prolonged overheating and moisture-induced aging of submarine cables macroscopically alter their distributed capacitance and parasitic inductance parameters. This causes the parallel resonance peak formed by the grid-side filter and the long-distance submarine cable to drift in the frequency domain (such resonances typically reside between the $11^{th} \sim 35^{th}$ harmonics, i.e., $550 \sim 1750$ Hz). This mid-frequency feature is also well below the 6.4 kHz Nyquist limit and is therefore clearly captured by the Transformer's multi-terminal envelope analyzer.

In summary, by deeply mining the implicit correlations within low/mid-frequency harmonic envelopes, the system overcomes the engineering hardware bottleneck of relying on expensive high-frequency sensors (e.g., acoustic emission instruments, vibrometers), making large-scale intelligent O&M for heavy offshore assets truly feasible economically.

VIII. Conclusion

By introducing a predictive asset management framework, this paper constructs an anomaly contagion analysis method based on "5-Level 7-Node" multi-terminal harmonics. Evaluating a two-stage hybrid deep learning architecture based on CNN and Transformer, we conclude that an architecture capable of processing spatio-temporal dependencies is best suited for tracking cross-terminal fault contagion in the 5-Level 7-Node system. The front-end CNN model is responsible for highly sensitive transient anomaly neural envelope triggering, while the back-end Transformer architecture deduces the dynamic evolution of faults based on historical time-series data and provides a quantitative estimation of the contagion delay. Comprehensive simulation experiments based on a Python digital twin and deep learning framework successfully demonstrate the feasibility of early warning under multiple typical scenarios, verifying that significant protective lead-time windows can be obtained by tracing multi-terminal harmonic fingerprint time-series, which substantially enhances the safe operation margins and lifecycles of critical offshore wind electrical assets. Future work will focus on integrating long-term field operational data to refine the absolute accuracy of the time-delay predictions.

References

[1] M. I. H. Tusar and B. R. Sarker, "Maintenance cost minimization models for offshore wind farms: A systematic and critical review," *International Journal of Energy Research*, vol. 46, no. 4, pp. 3739–3765, 2022, doi: 10.1002/er.7425.

[2] N. Alagha, A. S. M. Khairuddin, Z. N. Haitaamar, et al., "Artificial intelligence in wind turbine fault detection and diagnosis: Advances and perspectives," *Energies*, vol. 18, no. 7, p. 1680, 2025, doi: 10.3390/en18071680.

[3] C. V. Amaechi, A. Reda, I. M. Kgosiemang, et al., "Guidelines on asset management of offshore facilities for monitoring, sustainable maintenance, and safety practices," *Sensors*, vol. 22, no. 19, p. 7270, 2022, doi: 10.3390/s22197270.

[4] A. M. Nassef, M. A. Abdelkareem, H. M. Maghrabie, et al., "Review of metaheuristic optimization algorithms for power systems problems," *Sustainability*, vol. 15, no. 12, p. 9434, 2023, doi: 10.3390/su15129434.

[5] S. Zhu, W. Ma, Y. Li, et al., "Research on sub-health monitoring of equipment based on industrial big data technology," *Vibroengineering Procedia*, vol. 44, pp. 15–20, 2022, doi: 10.21595/vp.2022.22724.

[6] Y. Zeng, "Causal Auditing and Protection Paradigm for Sub-health Offshore Wind Assets based on Multi-terminal Harmonic Fingerprinting (v1.0.0)," *Zenodo*, 2026, doi: 10.5281/zenodo.20267143.

[7] Y. Zeng, "A Causal Auditing Paradigm for Sub-health Diagnosis of Offshore Wind Assets via Multi-terminal Harmonic Fingerprinting (V1.0.0)," *Zenodo*, 2026, doi: 10.5281/zenodo.20149720.

[8] M. Achouch, M. Dimitrova, K. Ziane, et al., "On predictive maintenance in industry 4.0: Overview, models, and challenges," *Applied Sciences*, vol. 12, no. 16, p. 8081, 2022, doi: 10.3390/app12168081.

[9] H. Fox, A. C. Pillai, D. Friedrich, et al., "A review of predictive and prescriptive offshore wind farm operation and maintenance," *Energies*, vol. 15, no. 2, p. 504, 2022, doi: 10.3390/en15020504.

[10] J. Pan, A. Kimmig, D. Wu, et al., "A systematic review of data-driven approaches to fault diagnosis and early warning," *Journal of Intelligent Manufacturing*, vol. 34, no. 8, pp. 3277–3304, 2023, doi: 10.1007/s10845-022-02020-0.

[11] X. Zhou, Q. Chen, L. Zhang, et al., "A Unified Transformer-Based Harmonic Detection Network for Distorted Power Systems," *Energies*, vol. 19, no. 3, p. 650, 2026, doi: 10.3390/en19030650.

[12] H. Xue, N. Yao, Q. Fan, et al., "Analysis of power system signal processing method based on deep convolutional neural network," *International Journal of High Speed Electronics and Systems*, vol. 34, no. 1, p. 2540223, 2024, doi: 10.1142/S0129156425402232.

[13] R. P. Dos Santos, J. P. Matos-Carvalho, and V. R. Q. Leithardt, "Deep learning in time series forecasting with transformer models and RNNs," *PeerJ Computer Science*, vol. 11, p. e3001, 2025, doi: 10.7717/peerj-cs.3001.

[14] M. L. Duc, P. Bilik, and R. Martinek, "Harmonics signal feature extraction techniques: A review," *Mathematics*, vol. 11, no. 8, p. 1877, 2023, doi: 10.3390/math11081877.

[15] R. Chen, D. Qin, and C. Liu, "Dynamic modelling and dynamic characteristics of wind turbine transmission gearbox-generator system electromechanical-rigid-flexible coupling," *Alexandria Engineering Journal*, vol. 65, pp. 307–325, 2023, doi: 10.1016/j.aej.2022.10.036.

[16] J. Li, Y. Lin, and S. Su, "Identifying critical nodes in power grids containing renewable energy based on electrical spreading probability," *International Journal of Electrical Power & Energy Systems*, vol. 154, p. 109431, 2023, doi: 10.1016/j.ijepes.2023.109431.

[17] N. Sharma, S. Tian, D. Chen, et al., "Impedance assessment of offshore wind farms," in *19th International Conference on AC and DC Power Transmission (ACDC 2023)*, IET, 2023, pp. 239–245, doi: 10.1049/icp.2023.1335.

[18] S. Tripathi and A. K. Jain, "Minimization of DC Bus Side Current Ripple in DFIG Supported DC Micro Grid," in *2024 IEEE International Conference on Power Electronics, Drives and Energy Systems (PEDES)*, IEEE, 2024, pp. 1–6, doi: 10.1109/PEDES61459.2024.10961395.

[19] H. Deng, J. Fang, Y. Qi, et al., "A generic voltage control for grid-forming converters with improved power loop dynamics," *IEEE Transactions on Industrial Electronics*, vol. 70, no. 4, pp. 3933–3943, 2022, doi: 10.1109/TIE.2022.3176308.

[20] F. Zhou, "Drive-train torsional vibration suppression of large scale PMSG-based WECS," *Protection and Control of Modern Power Systems*, vol. 7, no. 1, p. 37, 2022, doi: 10.1186/s41601-022-00257-8.

[21] Y. Ding and M. Jia, "Convolutional transformer: An enhanced attention mechanism architecture for remaining useful life estimation of bearings," *IEEE Transactions on Instrumentation and Measurement*, vol. 71, pp. 1–10, 2022, doi: 10.1109/TIM.2022.3181933.

[22] R. D. Frederiksen, G. Bocewicz, G. Radzki, et al., "Cost-effectiveness of predictive maintenance for offshore wind farms: A case study," *Energies*, vol. 17, no. 13, p. 3147, 2024, doi: 10.3390/en17133147.

[23] H. Meng, X. Liu, J. Xing, and E. Zio, "A method for economic evaluation of predictive maintenance technologies by integrating system dynamics and evolutionary game modelling," *Reliability Engineering & System Safety*, vol. 222, p. 108424, 2022, doi: 10.1016/j.ress.2022.108424.

[24] G. Van Houtven, "Economic value of flood forecasts and early warning systems: a review," *Natural Hazards Review*, vol. 25, no. 4, p. 03124002, 2024, doi: 10.1061/NHREFO.NHENG-1865.
[25] P. Papadopoulos, D. W. Coit, and A. A. Ezzat, "STOCHOS: Stochastic opportunistic maintenance scheduling for offshore wind farms," *IISE Transactions*, vol. 56, no. 12, pp. 1319–1335, 2024, doi: 10.1080/24725854.2023.2268713.
[26] K. Cho, K. Shao, and A. Mesbah, "Run-indexed time-varying Bayesian optimization with positional encoding for auto-tuning of controllers: Application to a plasma-assisted deposition process with run-to-run drifts," *Computers & Chemical Engineering*, vol. 185, p. 108653, 2024, doi: 10.1016/j.compchemeng.2024.108653.
[27] B. Guan, S. Wang, Q. Zhu, et al., "Thrust Bearing Faults Diagnosis Using Multiphase Current Signals With Sub-Nyquist Sampling," *IEEE/ASME Transactions on Mechatronics*, vol. 30, no. 1, pp. 1–10, 2025, doi: 10.1109/TMECH.2025.3543129.
[28] F. Pérez Carrasco, A. Fernández García, A. García, et al., "Cloud-Based Architecture for Hydrophone Data Acquisition and Processing of Surface and Underwater Vehicle Detection," *Journal of Marine Science and Engineering*, vol. 13, no. 8, p. 1455, 2025, doi: 10.3390/jmse13081455.
[29] Z. Mu, G. Tian, X. Feng, et al., "Aerodynamic performance degradation of offshore wind turbine blades under icing with varying angles of attack," *Ocean Engineering*, vol. 341, p. 122776, 2025, doi: 10.1016/j.oceaneng.2025.122776.
[30] L. Zou, Z. Liu, Q. Liu, et al., "Investigation of the Impact of XLPE Cable Ageing on Impedance Mismatch Characteristics and Unbalanced Behaviour in Hybrid Operation Systems," *High Voltage*, vol. 11, no. 2, pp. 268–280, 2026, doi: 10.1049/hve2.70106.